Journal of Scientific Computing (2020) 82:24
https://doi.org/10.1007/s10915-019-01109-8

Discontinuous Galerkin Methods for the Ostrovsky–Vakhnenko Equation

Qian Zhang[1] · **Yinhua Xia**[1]

Received: 27 July 2019 / Revised: 7 November 2019 / Accepted: 30 December 2019

Abstract
In this paper, we develop discontinuous Galerkin methods for the Ostrovsky–Vakhnenko (OV) equation, which yields the shock solutions and singular soliton solutions, such as peakon, cuspon and loop solitons. The OV equation has also been shown to have a bi-Hamiltonian structure. We directly develop the energy stable or Hamiltonian conservative discontinuous Galerkin schemes for the OV equation. Error estimates for the two energy stable schemes are also proved. For some singular solutions, including cuspon and loop soliton solutions, the hodograph transformation is adopted to transform the OV equation or the generalized OV system to the coupled dispersionless (CD) system. Subsequently, two discontinuous Galerkin schemes are constructed for the transformed CD system. Numerical experiments are provided to demonstrate the accuracy and capability of the proposed schemes, including shock solution and, peakon, cuspon and loop soliton solutions.

Keywords Discontinuous Galerkin method · Ostrovsky–Vakhnenko equation · Energy stable · Hamiltonian conservative · Hodograph transformation · Coupled dispersionless system

1 Introduction

In this paper, we study the initial-value problem of the Ostrovsky–Vakhnenko (OV) equation

$$\begin{cases} (u_t + uu_x)_x + \gamma u = 0, \quad x \in I = [a, b], \ t \in [0, T], \\ u_0(x) = u(x, 0), \end{cases} \tag{1.1}$$

Yinhua Xia: Research supported by NSFC Grant 11871449, and a Grant from Laboratory of Computational Physics (No. 6142A0502020817).

✉ Yinhua Xia
yhxia@ustc.edu.cn

Qian Zhang
gelee@mail.ustc.edu.cn

[1] School of Mathematical Sciences, University of Science and Technology of China, Hefei 230026, Anhui, People's Republic of China

Published online: 18 January 2020

where the initial datum u_0 satisfy the condition $\int_I u_0 dx = 0$ which guarantee the well-posedness of the OV equation [13]. This equation can be viewed as a particular limit of the generalized Korteweg–de Vries (KdV) equation

$$(u_t + uu_x + \beta u_{xxx})_x + \gamma u = 0. \tag{1.2}$$

Here, γ is a real constant which concerns the effect of background rotation by Coriolis force in small-amplitude long waves on a shallow fluid [13]. It generalizes the Korteweg–de Vries equation by the additional term γu. Although it has the same nonlinear term of the KdV equation, the dispersive terms are different. When $\beta = 0$, the Eq. (1.2) degenerates to (1.1) without high-frequency dispersion term. It can be viewed as a canonical asymptotic equation for nonlinear waves that are non-dispersive as their wavelength tends to zero [13]. The Eq. (1.1) is deduced by considering two asymptotic expansions of the shallow water equations, first with respect to the rotation frequency, and then with respect to the amplitude of the waves [13]. Vakhnenko uses (1.1) to describe the short-wave perturbations in a relaxing medium [28], and it also be used to model sound waves in a bubbly liquid. The Ostrovsky–Vakhnenko equation has two properties that appear to be generic,

- Travelling waves that exist only up to a maximum limiting amplitude,
- Limiting waves that have corners, i.e., a slope discontinuity.

The Eq. (1.1) is known under different names in some literatures, such as the reduced Ostrovsky equation, the Ostrovsky–Hunter equation, the short-wave equation and the Vakhnenko equation, in this paper, we call (1.1) as Ostrovsky–Vakhnenko equation.

Many mathematical properties of the OV equation have been studied recently, some well-posedness results in energy space can be found in [11,16,30]. About convergence results of solutions in the limit, $\gamma \to 0$ or $\beta \to 0$, we refer the readers to [17–19]. In a series of papers [21,28,29], the integrability of OV equation was established by deriving explicit solutions. Some exact solutions including periodic solution, and solitary traveling wave solution are investigated in [13,22,23]. Besides the classical smooth solution, in [12,13,20], the authors have discussed the condition for wave breaking (shock solution). Also, continuous solutions with discontinuous slope are solved numerically, i.e. peakon solution, by a finite difference scheme based on the Engquist–Osher scheme [7,25], and cuspon solution (continuous solution with infinite discontinuous derivative) through the hodograph transformation [8,9]. Meanwhile, a multiple-value solution so called loop soliton solution is also defined in [8,9] via the hodograph transformation.

In this paper, we investigate the Hamiltonian H and E (we also called it energy),

$$E = \int_I u^2 dx, \quad H = \int_I -\frac{1}{6}u^3 + \frac{1}{2}(\partial^{-1}u)^2 dx, \tag{1.3}$$

which is confirmed in [2]. The development of our numerical schemes are based on these two conservative quantities. As the conservative methods for KdV equation [3,14,43], Zakharov system [37], Schrödinger–KdV system [38], short pulse equation [44], etc., various conservative numerical schemes are proposed to "preserve structure". Usually, the structure preserving schemes can help reduce the phase error along the long time evolution. For example in [3,14,43], compared with dissipative schemes, the energy conservative or Hamiltonian conservative numerical schemes for the KdV equation have less phase errors or amplitude damping for long time approximations, especially in the low resolution cases.

The discontinuous Galerkin (DG) method was first introduced in 1973 by Reed and Hill in [24] for solving steady state linear hyperbolic equations. The important ingredient of this method is the design of suitable inter-element boundary treatments (so called numerical

fluxes) to obtain highly accurate and stable schemes in several situations. Within the DG framework, the method was extended to deal with derivatives of order higher than one, i.e., local discontinuous Galerkin (LDG) method. The first LDG method was introduced by Cockburn and Shu in [6] for solving convection–diffusion equation. Their work was motivated by the successful numerical experiments of Bassi and Rebay [1] for compressible Navier–Stokes equations. Later, Yan and Shu developed an LDG method for a general KdV type equation containing third order derivatives in [39], and they generalized the LDG method to PDEs with fourth and fifth spatial derivatives in [40]. Levy et al. [15] developed LDG methods for nonlinear dispersive equations that have compactly supported traveling wave solutions, the so-called compactons. More recently, Xu and Shu further generalized the LDG method to solve a series of nonlinear wave equations [31–34,42]. We refer to the review paper [36] of LDG methods for high-order time-dependent partial differential equations.

In this paper, we adopt the DG method as a spatial discretization to construct high order accurate numerical schemes for the OV equation. For general solutions, the energy stable schemes based on energy E that contain the non-integration scheme and the integration DG scheme are developed. The energy stable schemes work for the smooth, peakon and shock solutions. On the other hand, the Hamiltonian conservative DG scheme can handle the smooth, peakon solutions and preserve the Hamiltonian H. Correspondingly, integration method will bring a Hamiltonian integration DG scheme. In the implementation of the progress, compared with the non-integration DG method, the integration one avoids solving linear system at each time level so that it reduces the complexity of programs. For the time discretization, we use the so called total variation diminishing (TVD) or strong stability preserving (SSP) explicit Runge–Kutta methods in [10,26]. For some singular soliton solutions, we utilize the hodograph transformation to transform the OV equation to a coupled dispersionless (CD) type system, and then establish the DG scheme for the transformed CD system.

The paper is organized as follows. In Sect. 2, we directly construct two energy stable, Hamiltonian conservative and Hamiltonian integration DG schemes for the OV equation. We provide proofs of L^2 stability and Hamiltonian conservation, respectively. Suboptimal error estimates of the two energy stable schemes are also proved in this section. For some singular soliton solutions, including loop and cuspon solitons, we transform the OV equation to the CD system via the hodograph transformation in Sect. 3. Subsequently, two DG schemes are constructed for the CD system to obtain the numerical solutions for the OV equation indirectly. Some numerical experiments are presented in Sect. 4 to show the results of approximation. This paper is concluded in Sect. 5.

2 The DG Methods for the Ostrovsky–Vakhnenko Equation

2.1 Notations

We denote the mesh $\mathcal{T}_h$ by $I_j = [x_{j-\frac{1}{2}}, x_{j+\frac{1}{2}}]$ for $j = 1, \ldots, N$, where $x_{\frac{1}{2}} = a, x_{N+\frac{1}{2}} = b$ with the cell center denoted by $x_j = \frac{1}{2}(x_{j-\frac{1}{2}} + x_{j+\frac{1}{2}})$. The cell size is $\Delta x_j = x_{j+\frac{1}{2}} - x_{j-\frac{1}{2}}$ and $h = \max_{1\le j\le N} \Delta x_j$. The finite element space as the solution and test function space consists of piecewise polynomials

$$V_h^k = \{v : v|_{I_j} \in P^k(I_j); 1 \le j \le N\},$$

where $P^k(I_j)$ denotes the set of polynomial of degree up to k defined on the cell I_j. Notably, the functions in V_h^k are allowed to be discontinuous across cell interfaces. The values of

u at $x_{j+\frac{1}{2}}$ are denoted by $u^-_{j+\frac{1}{2}}$ and $u^+_{j+\frac{1}{2}}$, from the left cell I_j and the right cell I_{j+1}, respectively. Additionally, the jump of u is defined as $[\![u]\!] = u^+ - u^-$, the average of u as $\{u\} = \frac{1}{2}(u^+ + u^-)$.

After the hodograph transformation, the spatial variable change into y from x. We denote the mesh $\mathcal{T}_h'$ by $I_j' = [y_{j-\frac{1}{2}}, y_{j+\frac{1}{2}}]$ for $j = 1, \ldots, N$. As the same definition on variable x, we have $y_j, \Delta y_j, h' = \max_{1\le j\le N} \Delta y_j$. To simplify expressions, we adopt the round bracket and angle bracket for the L^2 inner product and boundary term on cell I_j

$$\begin{aligned} (u, v)_{I_j} &= \int_{I_j} uv dy, \\ < \hat{u}, v >_{I_j} &= \hat{u}_{j+\frac{1}{2}} v^-_{j+\frac{1}{2}} - \hat{u}_{j-\frac{1}{2}} v^+_{j-\frac{1}{2}} \end{aligned} \tag{2.1}$$

for one dimensional case.

2.2 The Energy Stable DG Schemes

In this section, we develop two DG schemes with energy stability, for smooth solutions, suboptimal order of accuracy $(k+\frac{1}{2})$-th is proved for these two DG schemes. To distinguish other DG schemes in this paper, we name them the energy stable non-integration scheme and energy stable integration scheme for the OV equation.

Before the numerical scheme, we need to illustrate that the equation we discrete actually is the integration form of (1.1), i.e.

$$u_t + \left(\frac{1}{2}u^2\right)_x + \gamma \partial_x^{-1} u = 0. \tag{2.2}$$

We divide the OV equation into a first order system

$$\begin{cases} u_t + \left(\frac{1}{2}u^2\right)_x + \gamma v = 0, \\ v_x = u, \end{cases} \tag{2.3}$$

with periodic boundary condition or Dirichlet boundary condition for u. An extra constraint for v is necessary to ensure the uniqueness of the Eq. (2.3). To enforce the conservation law $\frac{d}{dt}\int_I u dx = 0$, it results in the zero mean condition $\int_I v dx = 0$.

2.2.1 The DG Scheme for the OV Equation

To develop the DG scheme for the Eq. (2.3), we rewrite it into the following specific form

$$\begin{cases} u_t + \left(\frac{1}{2}u^2\right)_x + \gamma v = 0, & \text{(2.4a)} \\ v_x = u, & \text{(2.4b)} \\ \int_I v dx = 0. & \text{(2.4c)} \end{cases}$$

Scheme 1 For the Eq. (2.4), the energy stable non-integration DG scheme is formulated as follows:

$$\begin{cases} ((u_h)_t, \phi)_{I_j} + < \widehat{f(u_h)}, \phi >_{I_j} - (f(u_h), \phi_x)_{I_j} + \gamma(v_h - \bar{v}_h, \phi)_{I_j} = 0, & \text{(2.5a)} \\ < \widehat{v_h}, \varphi >_{I_j} - (v_h, \varphi_x)_{I_j} = (u_h, \varphi)_{I_j} & \text{(2.5b)} \end{cases}$$

where $f(u) = \frac{1}{2}u^2$, $\bar{v}_h = \frac{1}{b-a}\int_I v_h$. The "hat" terms in (2.5) are the so-called "numerical fluxes", which are functions defined on the cell boundary from integration by parts and should be designed based on different guiding principles for different PDEs to ensure the stability and local solvability of the intermediate variables. To introduce some dissipation of energy, we adopt the dissipative numerical flux as

$$\widehat{f(u_h)} = \widehat{f}(u_h^-, u_h^+) = \frac{1}{2}(f(u_h^+) + f(u_h^-) - \alpha(u_h^+ - u_h^-)),\ \alpha = \max_u \left|f'(u)\right|. \tag{2.6}$$

Here $\widehat{f}(u_h^-, u_h^+)$ is the local Lax–Friedrichs flux, and the maximum for the parameter α is taken over the range covered by u_h^- and u_h^+. The numerical flux $\widehat{v_h}$ depends on the sign of the parameter γ,

$$\widehat{v_h} = \begin{cases} v_h^-, & \gamma > 0, \\ v_h^+, & \gamma < 0, \end{cases}, \tag{2.7}$$

which comes from the stability analysis. Here we consider the periodic or Dirichlet boundary condition for u. The Dirichlet boundary condition for u is given by exact solution

$$(u_h)^-_{\frac{1}{2}} = u(a,t), \quad (u_h)^+_{N+\frac{1}{2}} = u(b,t). \tag{2.8}$$

We take the start-up boundary value for v_h as

$$\begin{aligned} &(v_h)^-_{\frac{1}{2}} = 0, \quad \gamma > 0, \\ &(v_h)^+_{N+\frac{1}{2}} = 0, \ \gamma < 0. \end{aligned} \tag{2.9}$$

In fact, the boundary value $(v_h)^-_{\frac{1}{2}}$ or $(v_h)^+_{N+\frac{1}{2}}$ can be an arbitrary constant. We finally aim at enforcing the zero mean condition by setting $v_h = v_h - \bar{v}_h$. Numerically, the energy stable non-integration DG scheme (2.5) with numerical fluxes (2.6) and (2.7) can achieve the $(k+1)$-th order of accuracy.

Scheme 2 Alternatively, we can integrate the equation $(v_h)_x = u_h$ directly instead of the DG scheme (2.5b). Therefore, the energy stable integration DG scheme is defined as: Find the numerical solutions $u_h \in V_h^k$, $v_h \in V_h^{k+1} \cap \mathbb{C}^0$, for all test functions $\phi \in V_h^k$, such that

$$\begin{cases} ((u_h)_t, \phi)_{I_j} + < \widehat{f(u_h)}, \phi >_{I_j} - (f(u_h), \phi_x)_{I_j} + \gamma(v_h - \bar{v}_h, \phi)_{I_j} = 0, & \text{(2.10a)} \\ v_h(x,t)\ |_{I_j} = v_h(x_{j+\frac{1}{2}}, t) - \displaystyle\int_x^{x_{j+\frac{1}{2}}} u_h(\xi, t)\, d\xi. & \text{(2.10b)} \end{cases}$$

The Eq. (2.10b) can also be replaced by

$$v_h(x,t)\ |_{I_j} = v_h(x_{j-\frac{1}{2}}, t) + \int_{x_{j-\frac{1}{2}}}^{x} u_h(\xi, t)\, d\xi, \tag{2.11}$$

which depends on the start-up value v_h we give,

$$\begin{aligned} &(v_h)_{N+\frac{1}{2}} = 0 \text{ for } (2.10b), \\ &(v_h)_{\frac{1}{2}} = 0 \text{ for } (2.11). \end{aligned} \tag{2.12}$$

The boundary condition for u is the same as Scheme 1. Numerically, this energy stable integration DG scheme (2.10) achieve the optimal accuracy for u as well as the energy stable non-integration DG scheme.

2.2.2 Algorithm Flowchart

In this part, we give some details related to the implementation of our numerical Schemes 1 and 2. We can see that the equation (2.5a), (2.10a) are identical. The main difference between Schemes 1 and 2 lies in (2.5b) and (2.10b) which we will explain in Step 1 respectively.

Step 1: First, we obtain v_h from u_h by (2.5b) in Scheme 1, or (2.10b), (2.11) in Scheme 2.

- In Scheme 1: From the equation (2.5b), we have the following matrix form,

$$\mathbf{A}\mathbf{v}_h = \mathbf{u}_h. \tag{2.13}$$

Here, $\mathbf{u}_h$, $\mathbf{v}_h$ are the vectors containing the degrees of freedom for u_h and v_h, respectively. The size of matrix $\mathbf{A}$ is $(N*(k+1)) \times (N*(k+1))$, N is the number of spatial cells and k is the degree of the approximate space V_h^k. Actually, we need a boundary condition for v_h to start up the numerical scheme. To enforce the zero mean condition (2.4c) for v_h, we set the boundary $(v_h)^-_{\frac{1}{2}} = 0$ for $\gamma > 0$ or $(v_h)^+_{N+\frac{1}{2}} = 0$ for $\gamma < 0$. According to the Eq. (2.5b), we can get v_h on each cell I_j. Subsequently, we enforce the zero mean condition by

$$v_h = v_h - \bar{v}_h, \tag{2.14}$$

where $\bar{v}_h = \frac{1}{b-a}\int_I v_h$.

Remark 2.1 If u is periodic, then v is periodic too. And then a start-up value on boundary is unnecessary. However, the linear system (2.13) is under-determined and the rank of $\mathbf{A}$ is $N*(k+1)-1$. Therefore, the zero mean condition will help determine the unique solution v_h, i.e. we obtain the v_h satisfied the zero mean condition directly.

- In Scheme 2: First, we set the start-up value in boundary of v_h, $v_h(x_{\frac{1}{2}}, t) = 0$ in (2.10b) or $v_h(x_{N+\frac{1}{2}}, t) = 0$ in (2.11). Next, v_h can be solved cell by cell. Finally, we can have the mean value $\bar{v}_h$. Following the same procedure with Scheme 1, we enforce the zero mean condition by setting $v_h = v_h - \bar{v}_h$.

Step 2: Substituting the new value $v_h = v_h - \bar{v}_h$ into the Eq. (2.5a) or (2.10a), we have

$$(\mathbf{u}_h)_t = \mathbf{res}(\mathbf{u_h}, \mathbf{v_h}).$$

By choosing a suitable ODE solver, such as explicit Runge–Kutta time discretization methods, we will finally implement these two numerical schemes.

2.2.3 Energy Stability

The energy stability of Schemes 1 and 2 are presented in Propositions 2.1 and 2.2, respectively. Both schemes can be proved energy stable.

Proposition 2.1 (Energy stability for Scheme 1) *The semi-discrete DG scheme (2.5) for the periodic problem with fluxes* (2.6), (2.7) *is a mass conservative and energy stable DG scheme, i.e.,*

$$\frac{d}{dt}\int_I u_h dx = 0, \quad \frac{d}{dt}E(u_h) = \frac{d}{dt}\int_I u_h^2 dx \le 0. \tag{2.15}$$

Proof First, we take the test function $\phi = 1$ in Eq. (2.5a), after summing up all intervals I_j, the mass conservativeness $\frac{d}{dt}\int_I u_h dx = 0$ can be obtained.

Next, we try to prove the energy stability by taking the test function $\phi = u_h, \varphi = \gamma v_h$ in scheme (2.5), thereafter, we have

$$((u_h)_t, u_h)_{I_j} + < \widehat{f(u_h)}, u_h >_{I_j} -(f(u_h), (u_h)_x)_{I_j} + \gamma(v_h - \bar{v}_h, u_h)_{I_j} = 0,$$
$$\gamma < \widehat{v_h}, v_h >_{I_j} -\gamma(v_h, (v_h)_x)_{I_j} = \gamma(u_h, v_h)_{I_j}.$$

After applying summation of the above-mentioned two equations, we get

$$((u_h)_t, u_h)_{I_j} - \gamma \bar{v}_h(u_h, 1)_{I_j} + \Phi_{j+\frac{1}{2}} - \Phi_{j-\frac{1}{2}} + \Theta_{j-\frac{1}{2}} = 0 \tag{2.16}$$

where the numerical entropy flux is

$$\Phi = \gamma \widehat{v_h}(v_h^-) - \frac{\gamma}{2}(v_h^-)^2 + \widehat{f}(u_h)u_h^- - F(u_h^-) \tag{2.17}$$

with $F(u) = \int^u f(u)du$, and the extra term Θ is given by

$$\begin{aligned}\Theta =& -\gamma \widehat{v_h}[\![v_h]\!] + \frac{\gamma}{2}[\![(v_h)^2]\!] - \widehat{f}(u_h)[\![u_h]\!] + [\![F(u_h)]\!] \\ =& \gamma(-\widehat{v_h} + \{v_h\})[\![v_h]\!] + (f(\xi) - \widehat{f(u_h)})[\![u_h]\!].\end{aligned} \tag{2.18}$$

The second equality (2.18) is yielded by the mean value theorem $[\![F(u_h)]\!] = f(\xi)[\![u_h]\!]$, where the value ξ is between u^- and u^+. The choice of $\widehat{v_h}$ (2.7) can guarantee that the first term of (2.18) is non-negative. According to the monotonicity of the numerical flux $f(\uparrow, \downarrow)$, we divide the above-mentioned equation into two cases:

$$u^- \le \xi \le u^+, \ (f(\xi) - \widehat{f}(u_h^-, u_h^+))[\![u]\!] \ge 0,$$
$$u^+ \le \xi \le u^-, \ (f(\xi) - \widehat{f}(u_h^-, u_h^+))[\![u]\!] \ge 0.$$

Thereafter, we find that the whole term Θ is non-negative. Owing to the conservation law $\frac{d}{dt}\int_I u_h = 0$ and initial data u_0 satisfied $(u_0, 1)_I = 0$, we have $(u_h, 1)_I = 0$. After summing up the cell entropy equalities (2.16) with periodic boundary condition, we have the energy stability as

$$(u_h, (u_h)_t)_I \le 0, \tag{2.19}$$

i.e., energy stability of the DG scheme (2.5) for the OV equation. □

Proposition 2.2 (Energy stability for Scheme 2) *The semi-discrete DG scheme* (2.10) *for the periodic problem with flux* (2.6) *is a mass conservative and energy stable scheme, i.e.,*

$$\frac{d}{dt}\int_I u_h dx = 0, \quad \frac{d}{dt}E(u_h) = \frac{d}{dt}\int_I u_h^2 dx \le 0. \tag{2.20}$$

Proof The proof for mass conservativeness is exactly the same as Scheme 1. Here, we just provide the proof for energy stability. We take test function $\phi = u_h$ in (2.10a),

$$((u_h)_t, u_h)_{I_j} + < \widehat{f(u_h)}, u_h >_{I_j} -(f(u_h), (u_h)_x)_{I_j} + \gamma(v_h, u_h)_{I_j} - \gamma \bar{v}_h(u_h, 1)_{I_j} = 0, \tag{2.21}$$

Additionally, following the idea of Proposition 2.1, we can have a stable property for the nonlinear term $f(u)$. There is an extra term $\gamma(v_h, u_h)_{I_j}$ required to be estimated. The Scheme 2, which is also called the integration DG method, is based on $(v_h)_x = u_h$, then

$$\gamma(v_h, u_h)_{I_j} = \gamma(v_h, (v_h)_x)_{I_j} = \frac{\gamma}{2}\left((v_h)^2_{j+\frac{1}{2}} - (v_h)^2_{j-\frac{1}{2}}\right). \tag{2.22}$$

Due to the continuity of v_h and periodic boundary condition, we obtain the result of L^2 stability after summing up the Eq. (2.21) over all cells,

$$\frac{d}{dt}E(u_h) = \frac{d}{dt}\int_I u_h^2 dx \leq 0. \tag{2.23}$$

□

2.2.4 Error Estimates

In this section, the a-priori error estimate of Schemes 1 (2.5) and 2 (2.10) will be stated. Referring to the procedure in [35,41], we will give some proofs in the subsequent descriptions. Without loss of generality, we let $\gamma = 1$ in this section.

Notations, projections, and auxiliary results

First, we make some conventions for different constants. Under different circumstances, these constants will have different values. Following the convention in [35,41], we use the same notation C denote a positive constant which is independent of h, but depends on the solution of the problem considered in this paper. Additionally, the notation C_* in [35,41] is used to denote the constants which are relevant to the maximum of $\left|f''\right|$ and $\left|f'''\right|$. In this paper, our nonlinear term is adopted as $f(u) = \frac{1}{2}u^2$, hence $f''' = 0$, i.e. C_* depends on maximum of $\left|f''\right|$.

In [41], Zhang and Shu proposed a key quantity to measure the difference between the physical flux and numerical flux. In [35], Xu and Shu apply it to "uniform dissipative flux", for completeness, we list the definition and relevant properties in the following lemma.

Lemma 2.3 [41] *For any piecewise smooth function $w \in L^2(I)$, on each boundary point, we define*

$$\alpha(\widehat{f}; w) \equiv \alpha(\widehat{f}; w^+, w^-) \triangleq \begin{cases} [\![w]\!]^{-1}(f(\{w\}) - \widehat{f}(w)), & [\![w]\!] \neq 0, \\ \frac{1}{2}\left|f'(\{w\})\right|, & [\![w]\!] = 0, \end{cases} \tag{2.24}$$

where $\widehat{f}(w) = \widehat{f}(w^-, w^+)$ is a monotone numerical scheme consistent with the given flux f. The quantity $\alpha(\widehat{f}; w)$ is non-negative and bounded for $\forall (w^-, w^+) \in \mathbb{R}^2$. Meanwhile, we obtain the following estimate

$$\frac{1}{2}\left|f'(\{w\})\right| \leq \alpha(\widehat{f}; w) + C_* \left|[\![w]\!]\right|,$$
$$-\frac{1}{8}\left|f''(\{w\})\right| [\![w]\!] \leq \alpha(\widehat{f}; w) + C_* \left|[\![w]\!]\right|^2.$$

In Sect. 2.2.4, the dissipative monotone numerical scheme is taken as Lax–Friedrichs flux (2.6). For the sake of expression, we denote

$$\alpha(\widehat{f}; w)[\![\phi]\!]^2 = \sum_{j=1}^{N} \alpha(\widehat{f}; w)_{j+\frac{1}{2}} [\![\phi]\!]^2_{j+\frac{1}{2}} \tag{2.25}$$

for $\forall w$ and ϕ.

Next, we will introduce some projection properties to be used later. The standard L^2 projection of a function ζ with $k+1$ continuous derivatives into space V_h^k, is denoted by $\mathcal{P}$, i.e., for each I_j

$$(\mathcal{P}\zeta - \zeta, \phi)_{I_j} = 0, \ \forall \phi \in P^k(I_j),$$

and the special projections $\mathcal{P}^{\pm}$ into V_h^k satisfy, for each I_j

$$(\mathcal{P}^+\zeta - \zeta, \phi)_{I_j} = 0, \ \forall \phi \in P^{k-1}(I_j), \ \text{and } \mathcal{P}^+\zeta\left(y^+_{j-\frac{1}{2}}\right) = \zeta\left(y_{j-\frac{1}{2}}\right),$$
$$(\mathcal{P}^-\zeta - \zeta, \phi)_{I_j} = 0, \ \forall \phi \in P^{k-1}(I_j), \ \text{and } \mathcal{P}^-\zeta\left(y^-_{j+\frac{1}{2}}\right) = \zeta\left(y_{j+\frac{1}{2}}\right).$$

For the projections mentioned above, it is easy to show [4] that

$$\left\|\zeta^e\right\|_{L^2(I)} + h^{\frac{1}{2}}\left\|\zeta^e\right\|_{L^\infty(I)} + h^{\frac{1}{2}}\left\|\zeta^e\right\|_{L^2(\partial I)} \le Ch^{k+1} \tag{2.26}$$

where $\zeta^e = \zeta - \mathcal{P}\zeta$ or $\zeta^e = \zeta - \mathcal{P}^{\pm}\zeta$.

Then some inverse inequalities of finite element space V_h^k will be applied in the subsequent proofs.

Lemma 2.4 [4] *For $\forall \omega \in V_h^k$, there exists a positive constant C which is dependent of ω, h, such that*

$$(i)\ \|\omega_x\|_{L^2(I)} \le Ch^{-1}\|\omega\|_{L^2(I)}, \ (ii)\ \|\omega\|_{L^2(\partial I)} \le Ch^{-\frac{1}{2}}\|\omega\|_{L^2(I)},$$
$$(iii)\ \|\omega\|_{L^\infty(I)} \le Ch^{-\frac{1}{2}}\|\omega\|_{L^2(I)}, \tag{2.27}$$

where $\|\omega\|_{L^2(\partial I)} = \sqrt{\sum_{j=1}^{N}(\omega^-_{j+\frac{1}{2}})^2 + (\omega^+_{j-\frac{1}{2}})^2}$.

Finally, to deal with the nonlinearity of the flux $f(u)$, we make a priori assumption that, there holds

$$\|u - u_h\|_{L^2(I)} \le h \tag{2.28}$$

for small enough h. We will verity the justification of this assumption at the end of the proof for the theorem we will propose subsequently. Suppose that the interpolation properties (2.26) hold , by the inverse inequality (iii) in (2.27), the assumption (2.28) yields the error of L^∞ norm

$$\|u - u_h\|_{L^\infty(I)} \le Ch^{\frac{1}{2}}, \ \|\mathcal{Q}u - u_h\|_{L^\infty(I)} \le Ch^{\frac{1}{2}} \tag{2.29}$$

where $\mathcal{Q} = \mathcal{P}$ or $\mathcal{Q} = \mathcal{P}^{\pm}$.

Error estimate of Scheme 1

For the Scheme 1, we have below theorem to demonstrate the result of convergence for smooth exact solutions.

Theorem 2.5 *It is assumed that the OV equation (2.3) with periodic boundary condition has a sufficiently smooth exact solution u. The numerical solution u_h with initial condition $u_h(x,0) = \mathcal{P}u(x,0)$ satisfies the semi-discrete DG scheme (2.5) with fluxes (2.6), (2.7). For regular partitions of $I = (a,b)$, and the finite element space V_h^k with $k \ge 1$, there holds the following error estimate for small enough h*

$$\|u - u_h\|_{L^2(I)} \le Ch^{k+\frac{1}{2}}. \tag{2.30}$$

Proof First, we give the error equation between the exact solution and numerical solution,

$$\begin{aligned}((u-u_h)_t,\phi)_{I_j}+<f(u)-\widehat{f(u_h)},\phi>_{I_j}-(f(u)-f(u_h),\phi_x)_{I_j}+(v-v_h,\phi)_{I_j}\\ +<v-\widehat{v_h},\varphi>_{I_j}-(v-v_h,\varphi_x)_{I_j}-(u-u_h,\varphi)_{I_j}=0,\end{aligned}\tag{2.31}$$

for all test functions $\phi,\varphi\in V_h^k$. Thereafter, we define two bilinear forms

$$\begin{aligned}&\mathcal{B}_j(u-u_h,v-v_h;\phi,\varphi)\\ &=((u-u_h)_t,\phi)_{I_j}+(v-v_h,\phi)_{I_j}+<v-\widehat{v_h},\varphi>_{I_j}-(v-v_h,\varphi_x)_{I_j}-(u-u_h,\varphi)_{I_j}\end{aligned}\tag{2.32}$$

and

$$\mathcal{H}_j(f;u,u_h,\phi)=(f(u)-f(u_h),\phi_x)_{I_j}-<f(u)-\widehat{f(u_h)},\phi>_{I_j}.\tag{2.33}$$

After applying summation over all cells I_j, the error equation is expressed by

$$\sum_{j=1}^{N}\mathcal{B}_j(u-u_h,v-v_h;\phi,\varphi)=\sum_{j=1}^{N}\mathcal{H}_j(f;u,u_h,\phi).\tag{2.34}$$

Introducing notations

$$\xi^u=\mathcal{P}u-u_h,\ \eta^u=\mathcal{P}u-u,\tag{2.35}$$

$$\xi^v=\mathcal{P}^-v-v_h,\ \eta^v=\mathcal{P}^-v-v,\tag{2.36}$$

and taking test functions $\phi=\xi^u,\varphi=\xi^v$, we have

$$\sum_{j=1}^{N}\mathcal{B}_j(\xi^u-\eta^u,\xi^v-\eta^v;\xi^u,\xi^v)=\sum_{j=1}^{N}\mathcal{H}_j(f;u,u_h,\xi^u).\tag{2.37}$$

Next, we analyze the bilinear forms $\mathcal{B}_j$ and $\mathcal{H}_j$, respectively. For bilinear form $\mathcal{B}_j$, the following equation holds by projection properties

$$\sum_{j=1}^{N}\mathcal{B}_j(\xi^u-\eta^u,\xi^v-\eta^v;\xi^u,\xi^v)=(\xi_t^u,\xi^u)_I+\sum_{j=1}^{N}[\![\xi^v]\!]^2_{j+\frac{1}{2}}-(\eta^v,\xi^u)_I.\tag{2.38}$$

For bilinear form $\mathcal{H}_j$, we follow the idea of [35,41] to present the estimate of $\mathcal{H}_j$,

$$\begin{aligned}\sum_{j=1}^{N}\mathcal{H}_j(f;u,u_h,\xi^u)&\le-\frac{1}{4}\alpha(\widehat{f};u_h)[\![\xi^u]\!]^2+(C+C_*h^{-1}\|u-u_h\|^2_{L^\infty(I)})h^{2k+1}\\ &+(C+C_*(\|\xi^u\|_{L^\infty(I)}+h^{-1}\|u-u_h\|^2_{L^\infty(I)}))\|\xi^u\|^2_{L^2(I)}.\end{aligned}\tag{2.39}$$

Finally, combining the estimate Eqs. (2.38) and (2.39), we obtain the final error estimate as follows,

$$\begin{aligned}&(\xi_t^u,\xi^u)_I+\frac{1}{4}\alpha(\widehat{f};u_h)[\![\xi^u]\!]^2+\sum_{j=1}^{N}[\![\xi^v]\!]^2_{j+\frac{1}{2}}\\ &\le(\eta^v,\xi^u)_I+(C+C_*h^{-1}\|u-u_h\|^2_{L^\infty(I)})h^{2k+1}\\ &+(C+C_*(\|\xi^u\|_{L^\infty(I)}+h^{-1}\|u-u_h\|^2_{L^\infty(I)}))\|\xi^u\|^2_{L^2(I)}.\end{aligned}$$

Using the Young's inequality, the priori assumption (2.29) and the interpolation properties (2.26), we get

$$\frac{1}{2}\frac{d}{dt}\left\|\xi^u\right\|^2_{L^2(I)} \leq C\left\|\xi^u\right\|^2_{L^2(I)} + Ch^{2k+1} + Ch^{2k+2}.$$

By the Gronwall's inequality with initial condition $u_h(x,0) = \mathcal{P}u(x,0)$, the equation becomes

$$\left\|\xi^u\right\|^2_{L^2(I)} \leq Ch^{2k+1}.$$

Therefore, the result of Theorem 2.5 is derived by triangle inequality and the interpolation inequality (2.26). Finally, for the completeness of the Theorem 2.5, we verify the validity of the a-priori assumption (2.28). Here, for the cases $k \geq 1$, we assume that $Ch^{k+\frac{1}{2}} \leq \frac{1}{2}h$ holds for sufficiently small h, where the constant C depends on the final time T. Subsequently, we set $t^* = \sup\{t : \|u(t) - u_h(t)\|_{L^2(I)} \leq h\}$, due to the continuity we have $\|u(t^*) - u_h(t^*)\|_{L^2(I)} = h$ if t^* is finite. However, our roof for Theorem 2.5 concluded that $\|u(t^*) - u_h(t^*)\|_{L^2(I)} \leq Ch^{k+\frac{1}{2}} \leq \frac{1}{2}h$ for any $t \leq t^*$. Then we get a contradiction if $t^* \leq T$. Therefore, this result $t^* > T$ implies that the a-prior assumption is validate. □

Error estimate of Scheme 2

For the Scheme 2, we also state the following error estimate for smooth exact solutions.

Theorem 2.6 *It is assumed that the OV equation (2.3) with periodic boundary condition has a sufficiently smooth exact solution u. The numerical solution u_h with initial condition $u_h(x,0) = \mathcal{P}u(x,0)$ satisfies the energy stable integration DG scheme (2.10). For regular partitions of $I = (a,b)$, and the finite element space V_h^k with $k \geq 1$, for adequately small h, there holds*

$$\|u - u_h\|_{L^2(I)} \leq Ch^{k+\frac{1}{2}}. \tag{2.40}$$

Proof Similarly, we give the error equations,

$$((u-u_h)_t, \phi)_{I_j} + < f(u) - \widehat{f(u_h)}, \phi >_{I_j} -(f(u) - f(u_h), \phi_x)_{I_j} + (v - v_h, \phi)_{I_j} = 0,$$
$$(v - v_h)_x = u - u_h$$

for any test function $\phi \in V_h^k$. Thereafter, we define another bilinear form

$$\tilde{\mathcal{B}}_j(u - u_h, v - v_h; \phi) = ((u-u_h)_t, \phi)_{I_j} + (v - v_h, \phi)_{I_j}.$$

After applying summation over all cells I_j, the error equations are expressed by

$$\sum_{j=1}^{N} \tilde{\mathcal{B}}_j(u - u_h, v - v_h; \phi) = \sum_{j=1}^{N} \mathcal{H}_j(f; u, u_h, \phi).$$

We define notations $\xi^u \in V_h^k, \xi^v \in V_h^{k+1}$ as follows

$$\xi^u = \mathcal{P}^- u - u_h,\ \eta^u = \mathcal{P}^- u - u,$$
$$\xi^v = \tilde{v} - v_h,\ \eta^v = \tilde{v} - v$$

where $\tilde{v}_x = \mathcal{P}^- u$, $\tilde{v} \in V_h^{k+1}$ and $\tilde{v}(a,t) = v(a,t)$. By the Cauchy–Schwarz inequality, and the following estimate holds

$$|(\tilde{v} - v)(x)| = \left| (\tilde{v} - v)(a) + \int_a^x (P^- u - u)(\zeta) d\zeta \right| \leq C \left\| P^- u - u \right\|_{L^2(I)}$$

which implies that η^v can be controlled by η^u,

$$\left\| \eta^v \right\|_{L^2(I)} \leq C \left\| \eta^u \right\|_{L^2(I)} \leq C h^{k+1}. \tag{2.41}$$

With the test functions $\phi = \xi^u \in V_h^k$, we have

$$\sum_{j=1}^{N} \tilde{\mathcal{B}}_j(\xi^u - \eta^u, \xi^v - \eta^v; \xi^u) = \sum_{j=1}^{N} \mathcal{H}_j(f; u, u_h, \xi^u).$$

For the bilinear form $\tilde{\mathcal{B}}_j$, the following equation holds

$$\begin{aligned}
\sum_{j=1}^{N} \tilde{\mathcal{B}}_j(\xi^u - \eta^u, \xi^v - \eta^v; \xi^u, \xi^v) &= (\xi_t^u, \xi^u)_I - (\eta_t^u, \xi^u)_I + \sum_{j=1}^{N} (\xi^v, \xi^u)_{I_j} - (\eta^v, \xi^u)_I \\
&= (\xi_t^u, \xi^u)_I + \sum_{j=1}^{N} [\![(\xi^v)^2]\!]_{j+\frac{1}{2}} - (\eta^v, \xi^u)_I \\
&= (\xi_t^u, \xi^u)_I - (\eta^v, \xi^u)_I.
\end{aligned} \tag{2.42}$$

Combining estimate Eqs. (2.42) and (2.39), we will obtain the final error estimate,

$$\begin{aligned}
&(\xi_t^u, \xi^u)_I + \frac{1}{4} \alpha(\hat{f}; u_h) [\![\xi^u]\!]^2 \\
&\quad \leq (\eta^v, \xi^u)_I + (C + C_* (\left\| \xi^u \right\|_{L^\infty(I)} + h^{-1} \left\| u - u_h \right\|_{L^\infty(I)}^2)) \left\| \xi^u \right\|_{L^2(I)}^2 \\
&\qquad + (C + C_* h^{-1} \left\| u - u_h \right\|_{L^\infty(I)}^2) h^{2k+1}.
\end{aligned} \tag{2.43}$$

Using the Young's inequality, the priori assumption (2.29) and error estimate (2.41), we get

$$\frac{1}{2} \frac{d}{dt} \left\| \xi^u \right\|_{L^2(I)}^2 \leq C \left\| \xi^u \right\|_{L^2(I)}^2 + C h^{2k+1} + C h^{2k+2}. \tag{2.44}$$

Utilized the Gronwall inequality with initial datum $u_h(x,0) = \mathcal{P} u(x,0)$, the equation becomes

$$\left\| \xi^u \right\|_{L^2(I)}^2 \leq C h^{2k+1}.$$

Thus the result of Theorem 2.6 can be derived by triangle inequality and the interpolation inequality (2.26). □

2.3 The Hamiltonian DG Method

In this section, we construct another two DG schemes, which base on the Hamiltonian H, including the Hamiltonian conservative DG scheme and the Hamiltonian integration scheme. In this section, the sign of the parameter γ has no effect for numerical schemes we proposed and the Hamiltonian conservativeness. Hence we simply take $\gamma = 1$.

2.3.1 The DG Scheme for the OV Equation

We rewrite the OV equation (2.3) as another first order system

$$\begin{cases} u_t + w_x + v = 0, \\ w = \frac{1}{2}u^2, \\ v_x = u, \end{cases} \tag{2.45}$$

where v satisfies the zero mean condition $\int_I v dx = 0$.

Scheme 3 The Hamiltonian conservative DG scheme is defined as: Find numerical solutions $u_h, v_h, w_h \in V_h^k$, for all test functions $\phi, \varphi, \psi \in V_h^k$, such that

$$\begin{cases} ((u_h)_t, \phi)_{I_j} + < \widehat{w_h}, \phi >_{I_j} -(w_h, \phi_x)_{I_j} + (v_h - \bar{v}_h, \phi)_{I_j} = 0, & \text{(2.46a)} \\ (w_h, \varphi)_{I_j} = \left(\frac{1}{2}u_h^2, \varphi\right)_{I_j}, & \text{(2.46b)} \\ < \widehat{v_h}, \psi >_{I_j} -(v_h, \psi_x)_{I_j} = (u_h, \psi)_{I_j}. & \text{(2.46c)} \end{cases}$$

The numerical fluxes are taken as

$$\widehat{w_h} = \{w_h\}, \quad \widehat{v_h} = \{v_h\}. \tag{2.47}$$

Here, for the Hamiltonian conservative DG scheme, the boundary condition is taken as periodic. Numerically, this scheme have optimal order of accuracy $(k+1)$-th for even k on odd number meshes, it does not work for the rest situations. We will explain the reason in the section of algorithm flowchart (Sect. 2.3.2).

Remark 2.2 The Hamiltonian conservative DG scheme (2.46) with numerical fluxes (2.47) cannot preserve the Hamiltonian H and energy E both. If we adjust numerical fluxes as

$$\widehat{w_h} = \begin{cases} \frac{[\![F(u_h)]\!]}{[\![u_h]\!]}, & [\![u_h]\!] \neq 0, \\ f(\{u_h\}), & [\![u_h]\!] = 0. \end{cases}, \quad \widehat{v_h} = \{v_h\} \tag{2.48}$$

with $F(u) = \int^u f(u)du$, then the scheme (2.46) is equivalent to the Scheme 1 and conservative for $E(u_h)$ only.

Remark 2.3 For some solutions without sufficient smoothness, like peakon solution which only owns first classical derivative, we modify the numerical fluxes in (2.47) as

$$\widehat{w_h} = \{w_h\} - \alpha[\![u]\!], \quad \widehat{v_h} = \{v_h\} \tag{2.49}$$

to stabilize the behavior of numerical scheme (2.46) for long time approximations. Here, the parameter α is the same as the definition in (2.6). We will apply it to the peakon solution in the section of numerical experiments.

Scheme 4 We can still deal $v_x = u$ by directly integrating it, similar to the method followed in Eq. (2.10b) or (2.11). To avoid unnecessary duplication, we do not repeat the process. This scheme based on (2.45) has similar numerical results with the Hamiltonian conservative DG scheme (2.46), but it avoids solving the linear system at each time level and reduce the complexity of programs, even though the Hamiltonian conservation cannot be proved theoretically. Hereafter, we name this method by the Hamiltonian integration scheme as well as Scheme 4. Numerically, this Hamiltonian integration scheme can achieve the k-th order for odd k, the $(k+1)$-th order for even k.

2.3.2 Algorithm Flowchart

The main difference between the Hamiltonian conservative DG scheme and the energy stable non-integration scheme in Sect. 2 is the numerical fluxes $\widehat{v_h}$. The $\widehat{v_h}$ for the energy stable non-integration DG scheme is one-side, so we just need a start-up value on boundary. However, for the Hamiltonian conservative DG scheme, $\widehat{v_h}$ is taken as $\{v_h\}$ which needs two start-up values in the numerical scheme. It cannot be achieved by our method in Step 1 of Scheme 1 in the Sect. 2.2.2.

In fact, the Hamiltonian conservative DG scheme can only be achieved on odd number meshes with even degree k of space V_h^k for periodic boundary on u and v. Only for this case, we have the linear system

$$\mathbf{A}\mathbf{v}_h = \mathbf{u}_h$$

came from the Eq. (2.46c) with rank $N * (k+1) - 1$. Added the extra constraint, the zero mean condition, the linear system can be solved uniquely. The next procedures are exactly the same as those of the energy stable non-integration scheme in Sect. 2.2.2.

There is few difference on algorithm between the Hamiltonian integration scheme and the energy stable integration scheme, so we just omit the detail.

2.3.3 Hamiltonian Conservation

Proposition 2.7 *The semi-discrete DG scheme (2.46) with fluxes (2.47) is a mass conservative and Hamiltonian conservative DG scheme that can preserve the mass and Hamiltonian H simultaneously*

$$\frac{d}{dt}\int_I u_h dx = 0, \quad \frac{d}{dt}H(u_h, v_h) = \frac{d}{dt}\int_I -\frac{1}{6}u_h^3 + \frac{1}{2}v_h^2 dx = 0. \tag{2.50}$$

Proof With the periodic boundary condition, we can obtain the conservation of mass after summing up the Eq. (2.46a) with $\phi = 1$.

Subsequently, we give the proof for the Hamiltonian conservativeness. We take the time derivative of the Eq. (2.46c) to obtain

$$< \widehat{(v_h)_t}, \eta >_{I_j} -((v_h)_t, \eta_x)_{I_j} = ((u_h)_t, \eta)_{I_j}. \tag{2.51}$$

As (2.46a), (2.46b), (2.51) hold true for any test function in space V_h^k, we choose

$$\phi = (v_h)_t, \ \varphi = (u_h)_t, \ \eta = w_h. \tag{2.52}$$

Using the selected fluxes and summing up the three above-mentioned Eqs. (2.46a), (2.46b) and (2.51), we have

$$\begin{aligned}&((u_h)_t, (v_h)_t)_{I_j} + < \widehat{w_h}, (v_h)_t >_{I_j} -(w_h, (v_h)_{tx})_{I_j} + (v_h, (v_h)_t)_{I_j} - \bar{v}_h((v_h)_t, 1)_{I_j} \\ &+ < \widehat{(v_h)_t}, w_h >_{I_j} -((v_h)_t, (w_h)_x)_{I_j} - \left(\frac{1}{2}u_h^2, (u_h)_t\right)_{I_j} = 0.\end{aligned} \tag{2.53}$$

To eliminate the extra term $((u_h)_t, (v_h)_t)_{I_j}$, we take the test function $\eta = (v_h)_t$ in Eq. (2.51), and obtain

$$< \widehat{(v_h)_t}, (v_h)_t >_{I_j} -((v_h)_t, (v_h)_{tx})_{I_j} = ((u_h)_t, (v_h)_t)_{I_j}. \tag{2.54}$$

Substituting Eq. (2.54) into (2.53), we finally get the following summation

$$< \widehat{(v_h)_t}, (v_h)_t >_{I_j} -((v_h)_t, (v_h)_{tx})_{I_j} + < \widehat{w_h}, (v_h)_t >_{I_j} -(w_h, (v_h)_{tx})_{I_j} + (v_h, (v_h)_t)_{I_j}$$

$$-\bar{v}_h((v_h)_t,1)_{I_j}+<\widehat{(v_h)_t},w_h>_{I_j}-((v_h)_t,(w_h)_x)_{I_j}-\left(\frac{1}{2}u_h^2,(u_h)_t\right)_{I_j}=0. \quad (2.55)$$

We rewrite the above-mentioned equation into its equivalence form

$$(v_h,(v_h)_t)_{I_j}-\left(\frac{1}{2}u_h^2,(u_h)_t\right)_{I_j}-\bar{v}_h((v_h)_t,1)_{I_j}+\Phi_{j+\frac{1}{2}}-\Phi_{j-\frac{1}{2}}+\Theta_{j-\frac{1}{2}}=0 \quad (2.56)$$

where the numerical entropy flux is given by

$$\Phi=\widehat{w_h}(v_h^-)_t+\widehat{(v_h)_t}w_h^--(v_h^-)_tw_h^-+\widehat{v_h}(v_h^-)-\frac{1}{2}(v_h^-)^2 \quad (2.57)$$

and the extra term Θ is

$$\Theta=-\widehat{w_h}[\![(v_h)_t]\!]-\widehat{(v_h)_t}[\![w_h]\!]+[\![w_h(v_h)_t]\!]-\widehat{v_h}[\![v_h]\!]+\frac{1}{2}[\![(v_h)^2]\!]=0. \quad (2.58)$$

Summed up the cell entropy equalities (2.56) with periodic boundary condition, the Hamiltonian conservation is proved

$$\left(-\frac{1}{2}(u_h)^2,(u_h)_t\right)_I+(v_h,(v_h)_t)_I=0, \quad (2.59)$$

i.e., Hamiltonian conservative DG scheme for the OV equation. □

3 The DG Methods Via the Hodograph Transformation

In this section, we solve the singular solutions of the OV equation (1.1) by transforming it into a new coupled dispersionless type equation (CD system). This type of methods that solve numerical solutions by hodograph transformations are also applied in [44] for the short pulse equation. Similar to the method followed in [44], a DG scheme and an integration DG scheme are constructed for the transformed CD system. After obtaining the numerical solutions of the CD system, the profiles of solutions for the OV equation are obtained.

First, we analyze a more general case, two-component OV system as

$$\begin{cases}(u_t+uu_x)_x+\gamma u=c(1-\rho), & (3.1a)\\ \rho_t+(\rho u)_x=0. & (3.1b)\end{cases}$$

where $u(x,t)$ denote the amplitude of waves and $\rho(x,t)$ is the density of medium. When $c=0$, the two-component OV system will degenerate to the OV equation.

Through the conservation laws (3.1b), according to the compatibility condition, we set

$$y_x=\rho,\ y_t=-\rho u,$$

i.e. the hodograph transformation

$$dx=\frac{1}{\rho}dy+uds,\ dt=ds. \quad (3.2)$$

In this way, we link the two-component OV system (3.1) with a new type CD system

$$\begin{cases}(\rho^{-1})_s=u_y,\\ \rho u_{ys}+\gamma u+c(\rho-1)=0.\end{cases} \quad (3.3)$$

For the sake of expression and computation, we make $q = 1/\rho$, then we have

$$\begin{cases} q_s = u_y, \\ u_{ys} + \gamma q u + c(1-q) = 0, \end{cases} \tag{3.4}$$

for which we will construct the DG schemes in the subsequent section.

Subsequently, the parametric representation of the solution for the two-component OV system (3.1) is given by

$$u = u(y,s), \ \rho = \rho(y,s), \tag{3.5}$$

$$x = x(y_0,s) + \int_{y_0}^{y} \frac{1}{\rho(\zeta,s)} d\zeta, \ t = s. \tag{3.6}$$

where y_0 is a real constant.

Remark 3.1 When the two-component OV system degenerates to the OV equation with $c = 0$ in (3.1), there is no explicit conservation law for us to construct a hodograph transformation. In this case, we follow the method mentioned in [8] by transforming the OV equation to its bilinear form under which we will obtain the explicit representation of variable ρ. And then we can convert the OV equation into the CD system by the hodograph transformation (3.2).

3.1 The DG Schemes for the CD System

In this section, two DG schemes are constructed for the CD system (3.4), including the DG scheme and the integration DG scheme, the specific forms of which will be provided in Schemes 5 and 6, respectively.

We rewrite (3.4) as a first order system

$$\begin{cases} q_s = \omega, \\ \omega_s = -\gamma q u - c(1-q), \\ \omega = u_y. \end{cases} \tag{3.7}$$

Scheme 5 The DG scheme for the CD system (3.4) is defined as follows: Find $q_h, u_h, \omega_h \in V_h^k$, such that,

$$\begin{cases} ((q_h)_s, \phi)_{I_j'} = (\omega_h, \phi)_{I_j'}, & \text{(3.8a)} \\ ((\omega_h)_s, \varphi)_{I_j'} = -(\gamma q_h u_h, \varphi)_{I_j'} - (c(1-q_h), \varphi)_{I_j'}, & \text{(3.8b)} \\ (\omega_h, \psi)_{I_j'} = < \widehat{u_h}, \psi >_{I_j'} - (u_h, \psi_y)_{I_j'}, & \text{(3.8c)} \end{cases}$$

for all test functions $\phi, \varphi, \psi \in V_h^k$. Here, the numerical flux is $\widehat{u_h} = u_h^+$. After solving the numerical solutions of the CD system, we can finally profile the singular solutions of the OV system.

Scheme 6 Under the same DG framework (3.7), we use integration scheme deal with the equation $u_y = \omega$. Here, we construct the integration DG scheme for the CD system (3.4): Find $q_h, \omega_h \in V_h^k$, $u_h \in V_h^{k+1} \cap \mathbb{C}^0$, such that

$$\begin{cases} ((q_h)_s, \phi)_{I_j'} = (\omega_h, \phi)_{I_j'}, & \text{(3.9a)} \\ ((\omega_h)_s, \varphi)_{I_j'} = -(\gamma q_h u_h, \varphi)_{I_j'} - (c(1-q_h), \varphi)_{I_j'}, & \text{(3.9b)} \\ u_h(y,s) \mid_{I_j} = u_h(y_{j+\frac{1}{2}}, s) - \int_{y}^{y_{j+\frac{1}{2}}} \omega_h(\xi, s)\, d\xi, & \text{(3.9c)} \end{cases}$$

Table 1 DG schemes proposed in this paper

S/N	Equation	Scheme
Scheme 1	OV equation	The energy stable non-integration DG scheme (2.5)
Scheme 2	OV equation	The energy stable integration DG scheme (2.10)
Scheme 3	OV equation	The Hamiltonian conservative DG scheme (2.46)
Scheme 4	OV equation	The Hamiltonian integration scheme
Scheme 5	CD system	The DG scheme for CD system (3.8)
Scheme 6	CD system	The integration DG scheme for CD system (3.9)

for all test functions $\phi, \varphi \in V_h^k$. Here, the boundary condition is taken as $u_h(y_{N+\frac{1}{2}}, s) = u(b, s)$. The primary difference between this integration DG scheme (3.9) and the DG scheme (3.8) is the finite element space that the numerical solution u_h belongs to. In this case, not only u_h is in V_h^{k+1} space, but u_h is continuous. Numerically, this integration DG scheme can achieve the $(k+2)$-th order of accuracy for u_h, and the $(k+1)$-th order for q_h, ω_h.

3.2 Algorithm Flowchart

In this section, the processes of Schemes 5 and 6 are listed as follows:

Step 1: From the Eqs. (3.8a), (3.8b), we have

$$(\mathbf{q}_h)_s = \mathbf{Res}(\boldsymbol{\omega}_h),$$
$$(\boldsymbol{\omega}_h)_s = \mathbf{Res}(\mathbf{u}_h, \mathbf{q}_h).$$

The vectors $\mathbf{u}_h, \mathbf{q}_h, \boldsymbol{\omega}_h$ denote the freedoms of numerical solutions u_h, q_h, ω_h. Explicit TVD/SSP Runge–Kutta method is used for solving ω_h, q_h.

Step 2: From (3.8c) or (3.9c), we need to solve the coefficients of u_h from ω_h. We also need a boundary condition for u_h to start up the numerical scheme. The Dirichelet boundary condition by exact solution u is considered here. We do not list further details.

Remark 3.2 After the hodograph transformation, the conservation law for u cannot hold under the new spatial coordinate y, for periodic boundary condition on u, the lack of an extra constraint will cause the under-determined linear system for solving u_h.

4 Numerical Experiments

In this section, some numerical experiments are presented to show the convergence rate and capability of our numerical schemes. The time discretization method is the fourth order explicit Runge–Kutta method [10,26]. We take the time step as $\Delta t = 0.1\Delta x$ with our uniform spatial meshes for all experiments. Different solutions of the OV equation are calculated in this part, including not only smooth, shock solution, but peakon, cuspon and loop soliton solutions. In order to distinguish our proposed schemes clearly, we review them by Table 1.

Example 4.1 **Smooth solution** In this example, a smooth solution is used to test the accuracy and convergence rate of our numerical schemes with periodic boundary condition. The initial condition is taken as

$$u_0(x) = \sin(x), \ x \in [0, 2\pi]. \tag{4.1}$$

Table 2 Example 4.1, Schemes 1 and 2: accuracy test for smooth solution u (4.2) at $T = 1$

	N	Scheme 1				Scheme 2			
		$\|u-u_h\|_{L^2}$	Order	$\|u-u_h\|_{L^\infty}$	Order	$\|u-u_h\|_{L^2}$	Order	$\|u-u_h\|_{L^\infty}$	Order
P^1	40	4.74E−04	–	3.39E−03	–	4.74E−04	–	3.35E−03	–
	80	1.18E−04	2.00	8.43E−04	2.01	1.18E−04	2.00	8.38E−04	2.00
	160	2.95E−05	2.00	2.10E−04	2.00	2.95E−05	2.00	2.10E−04	2.00
	320	7.36E−06	2.00	5.25E−05	2.00	7.37E−06	2.00	5.24E−05	2.00
P^2	40	1.45E−05	–	1.16E−04	–	1.44E−05	–	1.14E−04	–
	80	1.93E−06	2.91	1.91E−05	2.60	1.93E−06	2.90	1.90E−05	2.58
	160	2.56E−07	2.91	3.00E−06	2.66	2.56E−07	2.91	2.99E−06	2.67
	320	3.53E−08	2.86	4.08E−07	2.88	3.53E−08	2.86	4.07E−07	2.88

Table 3 Example 4.1, Schemes 3 and 4: accuracy test for smooth solution u (4.2) at $T = 1$

	N	Scheme 3				Scheme 4			
		$\|u-u_h\|_{L^2}$	Order	$\|u-u_h\|_{L^\infty}$	Order	$\|u-u_h\|_{L^2}$	Order	$\|u-u_h\|_{L^\infty}$	Order
P^1	41	–	–	–	–	1.29E−02	–	1.54E−01	–
	81	–	–	–	–	7.40E−03	0.82	1.35E−01	0.20
	161	–	–	–	–	3.92E−03	0.92	8.55E−02	0.66
	321	–	–	–	–	2.00E−03	0.98	4.82E−02	0.83
P^2	41	1.23E−05	–	9.32E−05	–	1.23E−05	–	9.34E−05	–
	81	1.18E−06	3.45	8.46E−06	3.52	1.18E−06	3.45	8.44E−06	3.53
	161	1.17E−07	3.37	1.07E−06	3.01	1.17E−07	3.37	1.07E−06	3.01
	321	1.18E−08	3.32	1.16E−07	3.22	1.18E−08	3.32	1.16E−07	3.22

We fix the exact solution as

$$u(x,t) = \sin(x+t), \tag{4.2}$$

we add a source term $sf = \cos 2(x+t)$ to make sure the equation holds, that is,

$$\left(u_t + \left(\frac{1}{2}u^2\right)_x\right)_x + u = sf. \tag{4.3}$$

We record the errors, orders of accuracy at time $T = 1$ for proposed DG schemes in Tables 2 and 3. On the one hand, for two energy stable DG schemes, the convergence rates of L^2 and L^∞ errors are both $(k+1)$-th order for the variable u. For the Hamiltonian conservative DG scheme, there is $(k+1)$-th order for even k on odd number meshes, the rest cases cannot be approximated by Scheme 3. For the Hamiltonian integration DG scheme, we obtain the k-th order for odd k, $(k+1)$-th order for even k. On the other hand, we can see that the numerical errors of non-integration and integration schemes are almost identical. The integration method is more efficient than the non-integration one owing to not solving the linear system at each time level.

In Table 4, we compare the energy stable non-integration scheme and integration DG scheme on the variable v, the integration DG scheme is one order higher than the non-integration scheme on the variable v. However, the final numerical solution u belongs to

Table 4 Example 4.1, Schemes 1 and 2: accuracy test for the derivative of solution $v = u_x$ (4.2) at $T = 1$

	N	Scheme 1				Scheme 2			
		$\|v - v_h\|_{L^2}$	Order	$\|v - v_h\|_{L^\infty}$	Order	$\|v - v_h\|_{L^2}$	Order	$\|v - v_h\|_{L^\infty}$	Order
P^1	40	3.80E−04	–	1.71E−03	–	1.97E−05	2.99	9.76E−05	2.97
	80	9.22E−05	2.04	3.94E−04	2.12	2.46E−06	3.00	1.22E−05	3.00
	160	2.30E−05	2.01	9.39E−05	2.07	3.08E−07	3.00	1.53E−06	3.00
	320	5.75E−06	2.00	2.29E−05	2.04	3.85E−08	3.00	1.90E−07	3.00
P^2	40	4.73E−06	–	2.39E−05	–	4.41E−07	3.90	3.25E−06	3.89
	80	5.76E−07	3.04	2.91E−06	3.04	2.62E−08	4.07	2.32E−07	3.81
	160	7.29E−08	2.98	3.76E−07	2.95	1.60E−09	4.03	1.38E−08	4.07
	320	9.15E−09	2.99	4.66E−08	3.01	1.09E−10	3.88	1.02E−09	3.76

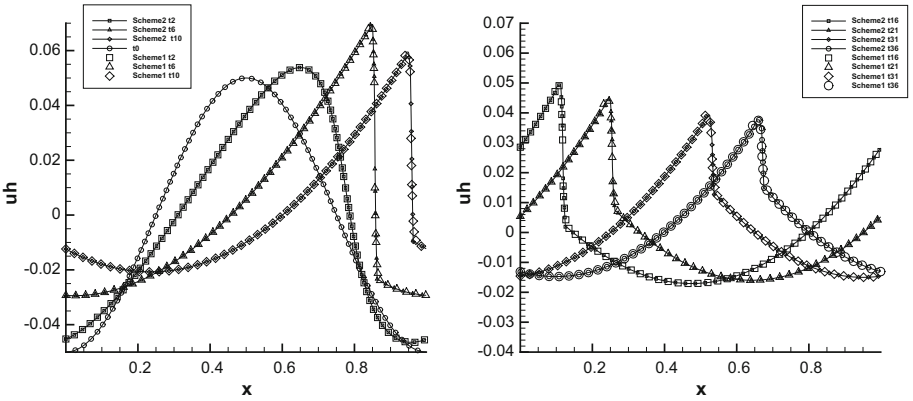

Fig. 1 Example 4.2, Schemes 1 and 2: the process of cosine initial condition (4.4) at different times $T = 0$ to $T = 36$ with the cells $N = 160$, P^2 elements

space V_h^k, therefore, the convergence rate for variable u is still $(k+1)$-th order rather than $(k+2)$-th.

Example 4.2 **Shock solution** In this example, we consider the smooth initial data

$$u_0(x) = -0.05\cos(2\pi x), \ x \in [0, 1], \tag{4.4}$$

for OV equation

$$\left(u_t + \left(\frac{1}{2}u^2\right)_x\right)_x - u = 0 \tag{4.5}$$

which will develop a shock in finite time. To eliminate the oscillation near the shock, we follow the idea of handling the shock solutions for conservation laws [5] to introduce a TVB limiter. Our numerical schemes can capture the shock without oscillation, see Fig. 1. We provide the approximation results of two energy stable DG schemes here. Because the lack of dissipation for nonlinear term $f(u)$, the Hamiltonian conservative scheme or the Hamiltonian integration scheme fails to model this shock solution.

Table 5 Example 4.3, Scheme 1: accuracy test for peakon solution (4.7) at $T = 36$

	N	$\|u - u_h\|_{L^2}$	Order	$\|u - u_h\|_{L^\infty}$	Order
P^1	20	1.86E−04	–	1.98E−03	–
	40	9.96E−05	0.90	1.27E−03	0.65
	80	4.65E−05	1.10	8.07E−04	0.65
	160	2.10E−05	1.15	5.00E−04	0.69
P^2	20	7.30E−05	–	6.78E−04	–
	40	3.22E−05	1.18	4.38E−04	0.63
	80	1.43E−05	1.18	3.11E−04	0.49
	160	6.22E−06	1.20	2.04E−04	0.61

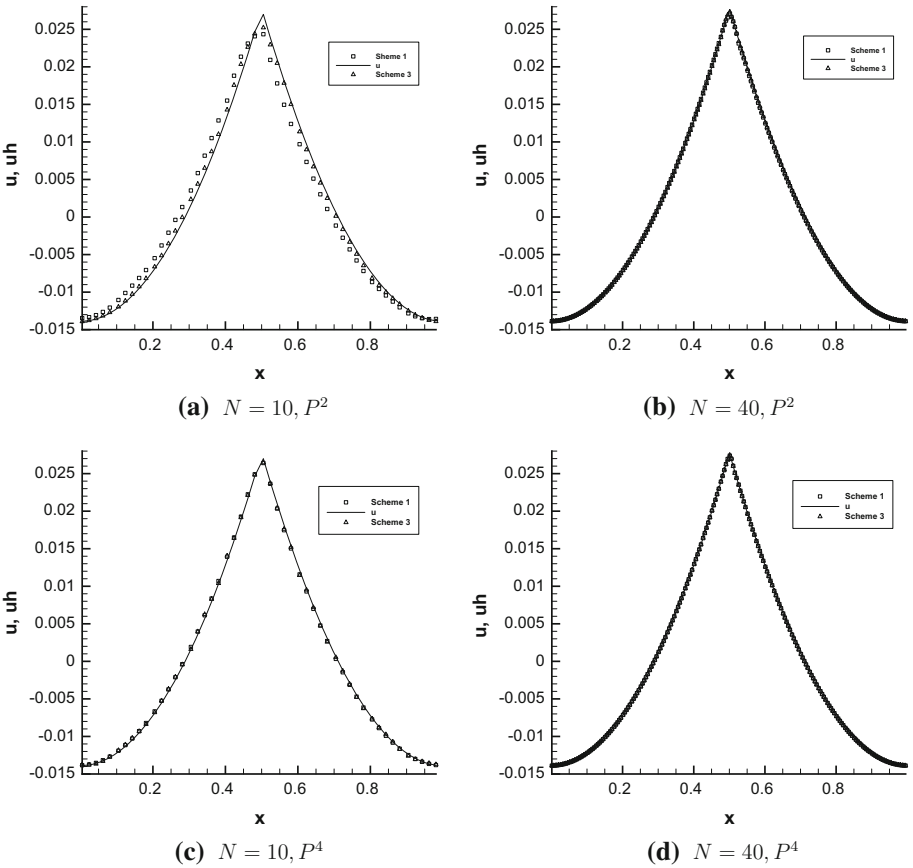

(a) $N = 10, P^2$ **(b)** $N = 40, P^2$

(c) $N = 10, P^4$ **(d)** $N = 40, P^4$

Fig. 2 Example 4.3, Schemes 1 and 3: Peakon solution (4.7) at T = 180

Table 6 Example 4.4, Scheme 5: accuracy test for the one-soliton solution (4.10) of the CD system (3.7) at $T = 1$, the computational domain is $[-20, 20]$, $k_1 = 1.0$, $c = 2.0$

	N	$\|u-u_h\|_{L^2}$	Order	$\|u-u_h\|_{\infty}$	Order	$\|\rho-\rho_h\|_{L^2}$	Order	$\|\rho-\rho_h\|_{\infty}$	Order
P^2	20	6.50E−03	–	7.13E−02	–	2.04E−02	–	2.93E−01	–
	40	1.14E−03	2.51	2.54E−02	1.49	2.32E−03	3.14	4.69E−02	2.64
	80	1.43E−04	3.00	2.55E−03	3.31	4.82E−04	2.27	8.73E−03	2.42
	160	2.05E−05	2.80	4.17E−04	2.62	6.38E−05	2.92	1.44E−03	2.60
	320	2.57E−06	2.99	5.20E−05	3.00	7.87E−06	3.02	1.75E−04	3.04
P^3	20	2.73E−03	–	3.56E−02	–	6.81E−03	–	8.69E−02	–
	40	2.69E−04	3.34	5.22E−03	2.77	9.20E−04	2.89	1.44E−02	2.59
	80	2.53E−05	3.41	5.00E−04	3.38	7.65E−05	3.59	1.50E−03	3.26
	160	1.35E−06	4.22	3.62E−05	3.79	4.12E−06	4.21	1.04E−04	3.86
	320	8.51E−08	3.99	2.39E−06	3.92	2.58E−07	4.00	7.10E−06	3.87

Table 7 Example 4.4, Scheme 6: accuracy test for the one-soliton solution (4.10) of the CD system (3.7) at $T = 1$, the computational domain is $[-20, 20]$, $k_1 = 1.0$, $c = 2.0$

	N	$\|u-u_h\|_{L^2}$	Order	$\|u-u_h\|_{\infty}$	Order	$\|\rho-\rho_h\|_{L^2}$	Order	$\|\rho-\rho_h\|_{\infty}$	Order
P^2	40	4.59E−04	–	7.01E−03	–	3.89E−03	–	5.44E−02	–
	80	2.31E−05	4.31	4.30E−04	4.03	5.39E−04	2.85	9.38E−03	2.54
	160	2.59E−06	3.16	6.49E−05	2.73	6.10E−05	3.14	1.21E−03	2.95
	320	1.65E−07	3.97	4.73E−06	3.78	7.71E−06	2.98	1.58E−04	2.94
	640	1.03E−08	3.99	3.02E−07	3.97	9.66E−07	3.00	1.97E−05	3.01
P^3	40	7.55E−05	–	1.26E−03	–	7.90E−04	–	9.93E−03	–
	80	6.90E−06	3.45	1.30E−04	3.28	3.36E−05	4.55	5.62E−04	4.14
	160	1.74E−07	5.31	4.19E−06	4.96	4.02E−06	3.06	9.16E−05	2.62
	320	5.52E−09	4.98	1.44E−07	4.86	2.55E−07	3.98	7.06E−06	3.70
	640	1.74E−10	4.98	4.50E−09	5.00	1.60E−08	4.00	4.54E−07	3.96

Example 4.3 **Peakon solution** This example is devoted to solve a well-known traveling wave solution of the OV equation with $\gamma = -1$, i.e. Eq. (4.5). We call the corner wave whose first order derivative is finite discontinuous as a peakon solution which is the limit case of a family of smooth traveling wave solution [13,22,27]. The initial data is given by

$$u_0(x) = \begin{cases} \frac{1}{6}(x-\frac{1}{2})^2 + \frac{1}{6}\left(x-\frac{1}{2}\right) + \frac{1}{36}, & x \in \left[0, \frac{1}{2}\right], \\ \frac{1}{6}\left(x-\frac{1}{2}\right)^2 - \frac{1}{6}\left(x-\frac{1}{2}\right) + \frac{1}{36}, & x \in \left[\frac{1}{2}, 1\right], \end{cases} \tag{4.6}$$

and the exact solution is

$$u(x,t) = u_0\big(x - \frac{t}{36}\big). \tag{4.7}$$

The solution at temporal time which equals multiple of 36 will return to its initial state after periods. First, we set the temporal time $T = 36$, the L^2, L^∞ errors and convergence rate of the energy stable non-integration scheme are contained in Table 5. Because of the lack of sufficient smoothness for the peakon solution, the convergence is the first order for L^2 norm, the $\frac{1}{2}$-th order for L^∞ norm which validates the results in [7]. In Fig. 2, two numerical

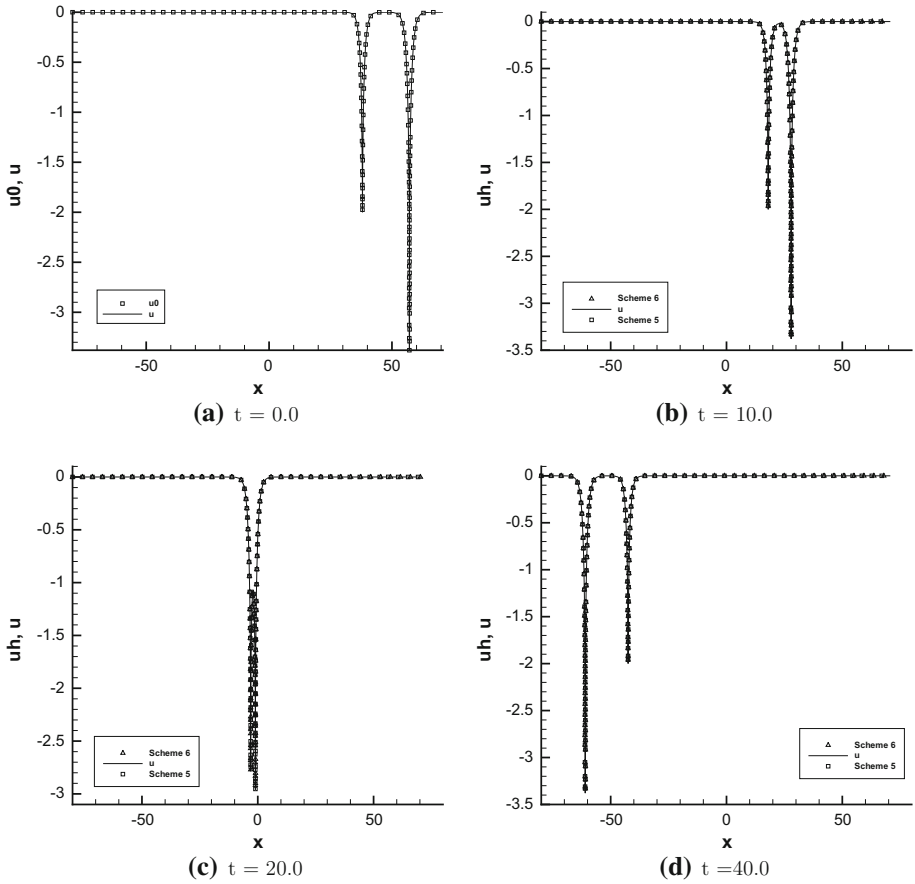

Fig. 3 Example 4.4, Schemes 5 and 6: the two-cuspon solution u of the OV system (4.8) with the cells $N = 320$, P^2 elements. The parameters are $k_1 = 2.0$, $k_2 = 2.6$, $c = -2.0$, $\eta_{i0} = -20k_i$

solutions at $T = 180$ are plotted. The Hamiltonian conservative DG scheme have some oscillations for long time approximation, hence we adopt the numerical fluxes (2.49) to stabilize this peakon solution. Here, this scheme is no longer Hamiltonian conservative. However, we can see that this Hamiltonian DG scheme has more accurate approximation than the energy stable non-integration DG scheme on same mesh. Without causing misunderstanding, we still denote this modified Hamiltonian DG scheme by Scheme 3 in Fig. 2. It can be seen that the finer mesh or higher order accuracy can help reduce the phase error and amplitude decay.

Example 4.4 **Loop and cuspon soliton solutions** This example is devoted to solve the loop and cuspon solutions for the OV equation and the two-component OV system with $\gamma = -3$,

$$\begin{cases} (u_t + uu_x)_x - 3u = c(1-\rho), \\ \rho_t + (\rho u)_x = 0 \end{cases} \tag{4.8}$$

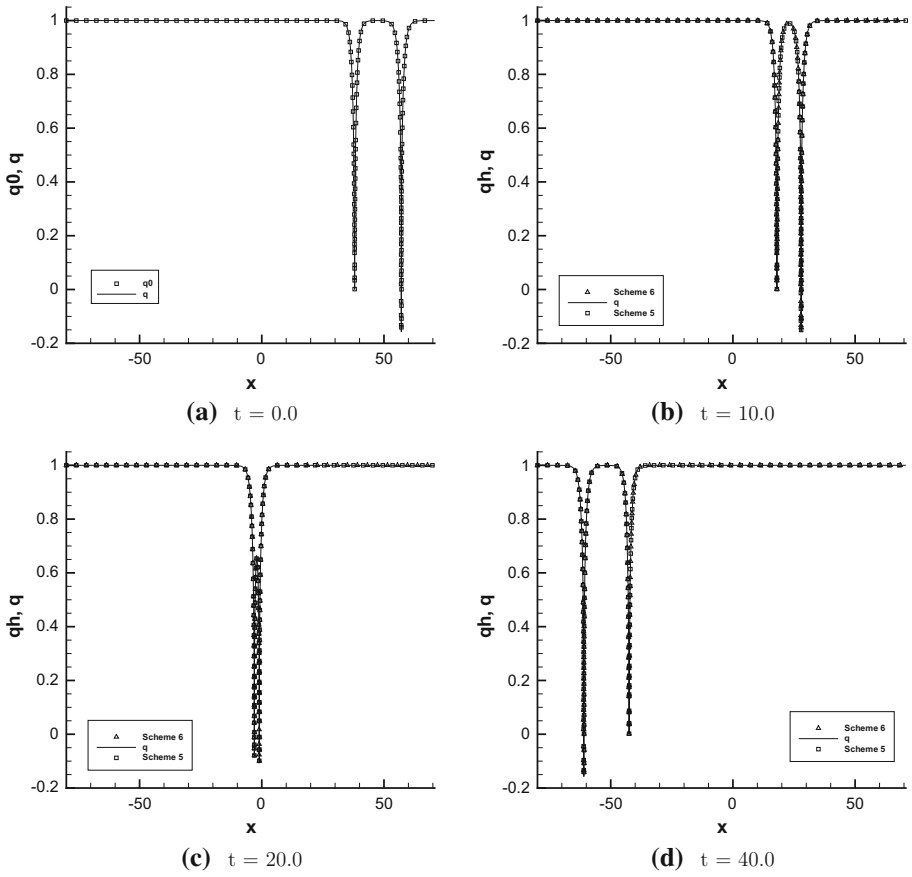

Fig. 4 Example 4.4, Schemes 5 and 6: the two-cuspon solution q of the OV system (4.8) with the cells $N = 320$, P^2 elements. The parameters are $k_1 = 2.0, k_2 = 2.6, c = -2.0, \eta_{i0} = -20k_i$

where $c = 0$, the system degenerates to the OV equation. We provide the exact solution of the OV system under the coordinate (y, s),

$$\begin{aligned} u(y,s) &= -2\ln(g)_{ss}, \\ \rho(y,s) &= (1 - 2(\ln g)_{ys})^{-1}, \\ x &= y - 2(\ln g)_s, \ t = s, \end{aligned} \tag{4.9}$$

which expresses the $\mathcal{N}$-soliton solutions, g is the Pfaffian polynomial.

First, we use the one-soliton solution to test the error and the convergence rate,

$$g = 1 + e^{\eta_1}, \ \eta_1 = k_1 s + \frac{3k_1}{k_1^2 - c} y + \eta_{10} \tag{4.10}$$

where $k_1 = 1.0, c = 2.0, \eta_{10} = 0.0$ are constants. The L^2, L^∞ errors and the convergence rates of two DG methods are listed in Tables 6, 7. We see that optimal error order can be both achieved for Schemes 5 and 6.

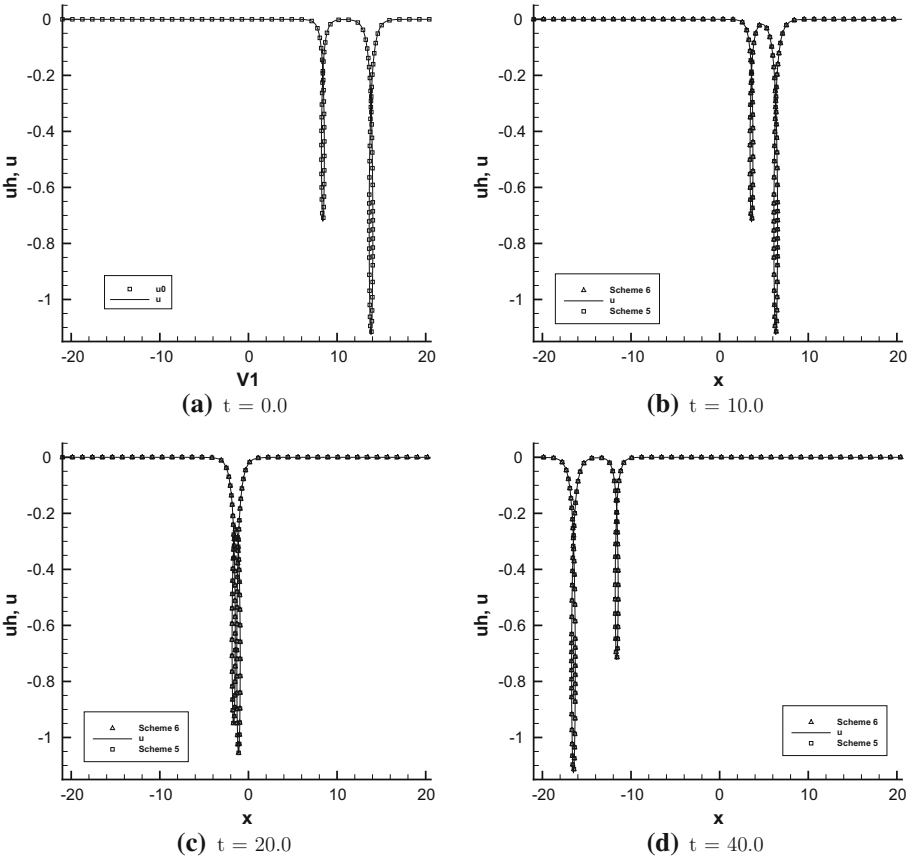

Fig. 5 Example 4.4, Schemes 5 and 6: the two-loop solution u of the OV system (4.8) with the cells $N = 320$, P^2 elements. The parameters are $k_1 = 1.2$, $k_2 = 1.5$, $c = 0.0$, $\eta_{i0} = -20k_i$

Next, we list the expression of the two-soliton solution

$$\begin{aligned} g &= 1 + e^{\eta_1} + e^{\eta_2} + b_{12}e^{\eta_1+\eta_2}, \\ \eta_i &= k_i s + \frac{3k_i}{k_i^2 - c} y + \eta_{i0}, \\ b_{12} &= \frac{(k_1 - k_2)^2(k_1^2 - k_1k_2 + k_2^2 - 3c)}{(k_1 + k_2)^2(k_1^2 + k_1k_2 + k_2^2 - 3c)}, \end{aligned} \tag{4.11}$$

where $c, k_i, \eta_{i0} = -20k_i$ are constants. Figures 3 and 4 display the elastic collision between two cuspon solitons in computational domain $[-80, 80]$. Referring to [9], the shape of solution depends on the choice of parameters k_i. In Fig. 5, we provide a 2-loop solution in $[-22, 20]$ for the OV equation. It can be seen that our numerical schemes have good resolutions for the cuspon and loop soliton solutions of the OV equation or the OV system.

5 Conclusion

In this paper, we presented the discontinuous Galerkin methods for the OV equation. These methods can be divided into two classes: direct and indirect. Direct methods consist of two energy stable, Hamiltonian conservative and Hamiltonian integration DG schemes for the OV equation. The L^2 stability and Hamiltonian conservativeness of the corresponding DG schemes are proved respectively. Based on the L^2 stability, we also give the suboptimal error estimates for two energy stable DG schemes. Indirect methods, composed of the DG scheme and the integration DG scheme for the CD system obtain the profile of solutions of the OV equation via the hodograph transformation. Numerical experiments are provided to demonstrate the accuracy and capability of the DG schemes, including shock solution, peakon, cuspon and loop soliton solutions, in addition to smooth solutions.

References

1. Bassi, F., Rebay, S.: A high-order accurate discontinuous finite element method for the numerical solution of the compressible Navier–Stokes equations. J. Comput. Phys. **131**(2), 267–279 (1997)
2. Brunelli, J.C., Sakovich, S.: Hamiltonian structures for the Ostrovsky–Vakhnenko equation. Commun. Nonlinear Sci. Numer. Simul. **18**(1), 56–62 (2013)
3. Bona, J., Chen, H., Karakashian, O., Xing, Y.: Conservative, discontinuous Galerkin methods for the generalized Korteweg–de Vries equation. Math. Comput. **82**(283), 1401–1432 (2013)
4. Ciarlet, P.G.: The Finite Element Method for Elliptic Problems. North Holland, Amsterdam (1975)
5. Cockburn, B., Lin, S.Y., Shu, C.-W.: TVB Runge–Kutta local projection discontinuous Galerkin finite element method for conservation laws III: one-dimensional systems. J. Comput. Phys. **84**(1), 90–113 (1989)
6. Cockburn, B., Shu, C.-W.: The local discontinuous Galerkin method for time-dependent convection–diffusion systems. SIAM J. Numer. Anal. **35**(6), 2440–2463 (1998)
7. Coclite, G.M., Ridder, J., Risebro, N.H.: A convergent finite difference scheme for the Ostrovsky–Hunter equation on a bounded domain. BIT Numer. Math. **57**(1), 93–122 (2017)
8. Feng, B.F., Maruno, K., Ohta, Y.: Integrable semi-discretizations of the reduced Ostrovsky equation. J. Phys. A: Math. Theor. **48**(13), 135203 (2015)
9. Feng, B.F., Maruno, K., Ohta, Y.: A two-component generalization of the reduced Ostrovsky equation and its integrable semi-discrete analogue. J. Phys. A: Math. Theor. **50**(5), 055201 (2017)
10. Gottlieb, S., Shu, C.-W., Tadmor, E.: Strong stability-preserving high-order time discretization methods. SIAM Rev. **43**(1), 89–112 (2001)
11. Gui, G., Liu, Y.: On the Cauchy problem for the Ostrovsky equation with positive dispersion. Commun. Partial Differ. Equ. **32**(12), 1895–1916 (2007)
12. Grimshaw, R.H.J., Helfrich, K., Johnson, E.R.: The reduced Ostrovsky equation: integrability and breaking. Stud. Appl. Math. **129**(4), 414–436 (2012)
13. Hunter, J.K.: Numerical solutions of some nonlinear dispersive wave equations. Lect. Appl. Math. **26**, 301–316 (1990)
14. Karakashian, O., Xing, Y.L.: A posteriori error estimates for conservative local discontinuous Galerkin methods for the generalized Korteweg–de Vries equation. Commun. Comput. Phys. **20**(01), 250–278 (2016)
15. Levy, D., Shu, C.-W., Yan, J.: Local discontinuous Galerkin methods for nonlinear dispersive equations. J. Comput. Phys. **196**(2), 751–772 (2004)
16. Linares, F., Milanés, A.: Local and global well-posedness for the Ostrovsky equation. J. Differ. Equ. **222**(2), 325–340 (2006)
17. Levandosky, S., Liu, Y.: Stability of solitary waves of a generalized Ostrovsky equation. SIAM J. Math. Anal. **38**(3), 985–1011 (2006)
18. Levandosky, S., Liu, Y.: Stability and weak rotation limit of solitary waves of the Ostrovsky equation. Discrete Contin. Dyn. Syst. Ser. B **7**(4), 793 (2007)
19. Liu, Y.: On the stability of solitary waves for the Ostrovsky equation. Q. Appl. Math. **65**(3), 571–589 (2007)

20. Liu, Y., Pelinovsky, D., Sakovich, A.: Wave breaking in the Ostrovsky–Hunter equation. SIAM J. Math. Anal. **42**(5), 1967–1985 (2010)
21. Parkes, E.J.: The stability of solutions of Vakhnenko's equation. J. Phys. A: Math. Gen. **26**(22), 6469 (1993)
22. Parkes, E.J.: Explicit solutions of the reduced Ostrovsky equation. Chaos Solitons Fractals **31**(3), 602–610 (2007)
23. Parkes, E.J.: Some periodic and solitary travelling-wave solutions of the short-pulse equation. Chaos Solitons Fractals **38**(1), 154–159 (2008)
24. Reed, W.H., Hill, T.R.: Triangular mesh methods for the neutron transport equation. Los Alamos Report LA-UR-73-479 (1973)
25. Ridder, J., Ruf, A.M.: A convergent finite difference scheme for the Ostrovsky–Hunter equation with Dirichlet boundary conditions. BIT Numer. Math. **59**, 1–22 (2018)
26. Shu, C.-W., Osher, S.: Efficient implementation of essentially non-oscillatory shock-capturing schemes. J. Comput. Phys. **77**(2), 439–471 (1988)
27. Stepanyants, Y.A.: On stationary solutions of the reduced Ostrovsky equation: periodic waves, compactons and compound solitons. Chaos Solitons Fractals **28**(1), 193–204 (2006)
28. Vakhnenko, V.A.: Solitons in a nonlinear model medium. J. Phys. A: Math. Gen. **25**(15), 4181 (1992)
29. Vakhnenko, V.O., Parkes, E.J.: The two loop soliton solution of the Vakhnenko equation. Nonlinearity **11**(6), 1457 (1998)
30. Varlamov, V., Liu, Y.: Cauchy problem for the Ostrovsky equation. Discrete Contin. Dyn. Syst.-A **10**(3), 731–753 (2004)
31. Xu, Y., Shu, C.-W.: Local discontinuous Galerkin methods for three classes of nonlinear wave equations. J. Comput. Math. **22**, 250–274 (2004)
32. Xu, Y., Shu, C.-W.: Local discontinuous Galerkin methods for nonlinear Schrödinger equations. J. Comput. Phys. **205**(1), 72–97 (2005)
33. Xu, Y., Shu, C.-W.: Local discontinuous Galerkin methods for two classes of two-dimensional nonlinear wave equations. Physica D **208**(1), 21–58 (2005)
34. Xu, Y., Shu, C.-W.: Local discontinuous Galerkin methods for the Kuramoto–Sivashinsky equations and the Ito-type coupled KdV equations. Comput. Methods Appl. Mech. Eng. **195**(25), 3430–3447 (2006)
35. Xu, Y., Shu, C.-W.: Error estimates of the semi-discrete local discontinuous Galerkin method for nonlinear convection–diffusion and KdV equations. Comput. Methods Appl. Mech. Eng. **196**(37–40), 3805–3822 (2007)
36. Xu, Y., Shu, C.-W.: Local discontinuous Galerkin methods for high-order time-dependent partial differential equations. Commun. Comput. Phys. **7**, 1–46 (2010)
37. Xia, Y., Xu, Y., Shu, C.-W.: Local discontinuous Galerkin methods for the generalized Zakharov system. J. Comput. Phys. **229**(4), 1238–1259 (2010)
38. Xia, Y., Xu, Y.: A conservative local discontinuous Galerkin method for the Schrödinger–KdV system. Commun. Comput. Phys. **15**(4), 1091–1107 (2014)
39. Yan, J., Shu, C.-W.: A local discontinuous Galerkin method for KdV type equations. SIAM J. Numer. Anal. **40**(2), 769–791 (2002)
40. Yan, J., Shu, C.-W.: Local discontinuous Galerkin methods for partial differential equations with higher order derivatives. J. Sci. Comput. **17**(1–4), 27–47 (2002)
41. Zhang, Q., Shu, C.-W.: Error estimates to smooth solutions of Runge–Kutta discontinuous Galerkin methods for scalar conservation laws. SIAM J. Numer. Anal. **42**(2), 641–666 (2004)
42. Zhang, C., Xu, Y., Xia, Y.: Local discontinuous Galerkin methods for the μ-Camassa–Holm and μ-Degasperis–Procesi equations. J. Sci. Comput. **79**, 1294–1334 (2019)
43. Zhang, Q., Xia, Y.: Conservative and dissipative local discontinuous Galerkin methods for Korteweg–de Vries type equations. Commun. Comput. Phys. **25**, 532–563 (2019)
44. Zhang, Q., Xia, Y.: Discontinuous Galerkin methods for short pulse type equations via hodograph transformations. J. Comput. Phys. **399**, 108928 (2019)